Noise Analysis and Modulation Optimization for Nonlinear Visible Light Communication System With Signal-Dependent Noise

Jiaqi Wei, Yuan Wang, Chen Gong, *Senior Member, IEEE*, and Nuo Huang

***Abstract*—This article investigates the characteristics of the signal-dependent noise (SDN) and corresponding modulation design in nonlinear visible light communication (VLC) systems. We first provide the noise model including SDN and signal-independent noise (SIDN) components. Then, we conduct three groups of comparative experiments to explore the noise characteristics in real VLC systems. Experimental results show that the dominance of SDN or SIDN is related to the linearity of VLC system. In a highly linear VLC system, the noise significantly increases with the signal strength. While in a VLC system with nonlinear devices, large nonlinear noise may make SDN less obvious. Based on the experimental results, a modulation optimization method is proposed for the VLC system with SDN. The symbol error rate (SER) of the optimized modulation is much lower than that of the uniform modulation in flat channel. Furthermore, we explore the effect of SDN on linear minimum mean square error (LMMSE) equalization. Simulation results show that the root mean square error of symbol estimation adopting LMMSE equalization is positively correlated with the modulation level. Moreover, the optimized modulation also outperforms the uniform modulation in the inter-symbol interference channel.**

***Index Terms*—Modulation optimization, nonlinear system, signal-dependent noise, visible light communication.**

I. Introduction

In THE past few decades, visible light communication (VLC) technology has received extensive attentions due to its distinct advantages such as low cost, no electromagnetic radiation and license-free bandwidth [1]. Utilizing light-emitting diode (LED) as the transmitter, VLC can simultaneously realize illumination and high-speed communication [2]. VLC is considered as an effective supplement to radio frequency (RF) communication, especially for in indoor scenarios.

Typically, avalanche photodiodes (APDs) are desirable receivers in VLC system, which converts optical signal into electrical signal with high sensitivity and response speed. Compared with photodiode (PD), APD effectively amplifies the signal via the avalanche multiplication. However, APD brings a specific problem to VLC: there can be signal-dependent noise (SDN) in the APD output besides the signal-independent noise (SIDN). These two types of noise are considered to be independent of each other. SDN mainly includes shot noise which is caused by the discreteness of electrons or photons and positively related to the signal strength [3].

Many studies have theoretically investigated the effect of SDN on the communication performance. The constellation distortion introduced by SDN for VLC systems has led to notable performance degradation [4]. SDN also negatively affects the channel estimation bound and the receiver's bit error rate (BER) performances [5], [6]. Therefore, in the presence of SDN, the optimal receiver, modulation and coding schemes need to be redesigned accordingly. By optimizing decoding thresholds, the modified minimum sum algorithm with a regular (3,6) low-density parity check (LDPC) code can achieve 0.7 dB gain over the scheme designed for only SIDN [7]. In works [8] and [9], the capacity bounds under peak-power and average-power constraints were derived for VLC channel models with SDN. Unlike the classical additive white Gaussian noise channels, the capacity in the SDN channels does not necessarily increase by reducing the noise variance [10]. Under certain technical conditions, the capacity-achieved distribution is proven to be a discrete input distribution with a finite number of mass points [11].

Modulation design is an effective way to improve communication performance, which is crucial for VLC system with SDN. There are many works focusing on quadrature amplitude modulation (QAM) design in VLC [12], [13]. However, SDN acts on time-domain waveforms so that existing modulation designs for SDN are mainly applied to pulse amplitude modulation (PAM) scheme. In [14], constellation and threshold values are optimized jointly to minimize the approximated detection error rate. Because the minimum Euclidian distance (MED) rule is no longer optimal for system with SDN, a linear combination of the minimum and maximum Euclidean distance is considered to attain a good power and error balance [15], [16]. To achieve the BER of 10^{-1}, such method could achieve a SNR gain of about 2.43 dB compared with MED based constellation design result for a sparse code multiple access (SCMA) based VLC downlink. Work [17] proposes an effective constellation design approach in

Manuscript received 15 July 2023; revised 17 September 2023; accepted 6 October 2023. Date of publication 9 October 2023; date of current version 19 October 2023. This work was supported in part by the National Natural Science Foundation of China under Grants 62331024, 62171428 and 62101526 and in part by the Fundamental Research Funds for the Central Universities under Grant KY2100000118. *(Corresponding author: Chen Gong; Nuo Huang.)*

The authors are with the CAS Key Laboratory of Wireless-Optical Communications, School of Information Science and Technology, University of Science and Technology of China, Hefei 230027, China (e-mail: kellyway@mail.ustc.edu.cn; wangy001@mail.ustc.edu.cn; cgong821@ustc.edu.cn; huangnuo@ustc.edu.cn).

Digital Object Identifier 10.1109/JPHOT.2023.3323139

a two-dimensional signal space, which provides extra freedom for constellation than that of one-dimensional.

In practical VLC systems, LEDs show significant nonlinearity during the electrical-to-optical (E/O) conversion. Such characteristic affects the noise model at the receiver. Existing work mainly considers two types of LED nonlinearities, including signal clipping and smooth transition. There is a threshold for the LED driving voltage, below which LED will not emit light. On the other hand, clipping occurs once the driving voltage exceeds the linear region of the LED. The model and impact of LED nonlinear response on BER performance are demonstrated in [18]. Work [19] optimized the communication performance based on the signal clipping model. Rapps model is typically adopted to represent the smooth transition characteristic and the knee factor is set to fit the smoothness [20]. Besides nonlinearities, LED exhibits low-pass frequency response limited by intrinsic properties such as carrier life time and RC time constant [21], [22]. The low-pass nature of LED results in inter-symbol interference (ISI) and plagues the VLC systems. There has been some works on ISI mitigation [23], [24].

In this work, we focus on the SDN in nonlinear VLC systems, and the major contributions can be summarized as follows. First, we propose the channel model for a typical indoor VLC system with nonlinear devices. Then, we explore the noise variance by comparative experiments, and analyzed the SDN and SIDN components. Experimental results show that the influence of SDN depends on the system linearity. Finally, we propose a modulation design method for the VLC system with SDN, and explore the effect of SDN on linear minimum mean square error (LMMSE) equalization. It is shown that the proposed modulation leads to lower symbol error rate (SER) than the uniform modulation in both flat and ISI channels.

The remainder of this article is organized as follows. A typical VLC system model is described in Section II. Section III presents the experimental results and analysis on SDN. Section IV provides a modulation design method to minimize the SER of VLC systems with SDN. Finally, we conclude this work in Section V.

A. Notation

Vectors and matrices are denoted by lower-case bold and capital bold letters. $(\cdot)^T$ and $(\cdot)^{-1}$ denote the transpose, inverse operators, respectively. diag$(\cdot)$ creates a diagonal matrix with the given elements. $\mathbb{E}\{\cdot\}$ and $\mathbb{D}\{\cdot\}$ denote the expectation and variance. The identity matrix is expressed as $\boldsymbol{I}$. $\mathcal{N}(\mu, \sigma^2)$ denotes a Gaussian distribution having mean μ and variance σ^2. $P(y|x)$ is the conditional probability of y given x.

II. System Model

A. Nonlinear Devices

Consider an indoor VLC system, as shown in Fig. 1. At the transmitter, the direct current (DC) and alternating current (AC) signals are combined by a signal coupler to drive the LED. The signal coupler may cause loss and distortion to the signal waveform. During the E/O conversion of LED, the output optical power also shows nonlinearity with the input electrical power. At the receiver, the APD converts the received optical signal into an electrical signal, which is further amplified by a low noise amplifier (LNA). The LNA design involves the tradeoffs between gain, linearity, and power dissipation, so LNA is not perfectly linear for input signal [25]. Finally, analog-to-digital converter (ADC) is adopted to convert the continuous waveform into a discrete digital signal for the subsequent signal processing.

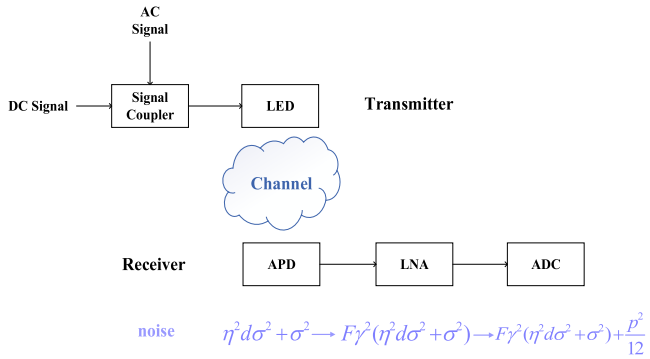

Fig. 1. Block diagram of the considered VLC system.

Denoting the APD input signal by d, the output noise variance is $\eta^2\, d\sigma^2 + \sigma^2$, where σ^2 is the SIDN variance, and η^2 characterizes the relative strength of SDN with respect to SIDN. Assume that the LNA amplifies the amplitude of APD output by γ times. The noise figure of LNA is defined as the ratio of input signal-to-noise ratio (SNR) to output SNR [26], i.e.,

$$F = \frac{SNR_{\text{in}}}{SNR_{\text{out}}} = \frac{S_{\text{in}}/N_{\text{in}}}{S_{\text{in}}\gamma^2/N_{\text{out}}} = \frac{N_{\text{out}}}{\gamma^2 N_{\text{in}}}, \tag{1}$$

where $N_{\text{in}} = \eta^2\, d\sigma^2 + \sigma^2$ is the input noise variance of LNA, and $N_{\text{out}} = F\gamma^2 N_{\text{in}}$ is the output noise variance of LNA. The noise figure F is typically adopted to evaluate the performance of amplifier. Lower F implies better performance. Generally, the output noise of LNA is still a Gaussian random variable.

The ADC converts the amplified signal into the digital signal, and its quantization errors are considered to occur at any point within $\pm\frac{p}{2}$ with equal probability, where $p > 0$ denotes one least significant bit (LSB) [27]. Then, the quantization noise variance is $\frac{p^2}{12}$.

B. Nonlinear System Model

Let x denote the zero-mean data symbol. To guarantee the signal non-negativity in the intensity modulation/direct detection (IM/DD)-based VLC system, a DC bias d_c is firstly added to x, and then a zero-level clipping is performed on signal $x + d_c$, yielding the non-negative transmitted signal s. According to the Bussgang theorem, the transmitted signal can be modeled as

$$s = \alpha x + \Delta x, \tag{2}$$

where $\alpha = \frac{\mathbb{E}[sx]}{\mathbb{E}[x^2]}$ is the attenuation factor, Δx is the distortion term uncorrelated with x [28].

According to the description in Section II-A, the received signal can be expressed as

$$\begin{aligned} y &= hs + \sqrt{hs}n_s + n_t + \Delta s \\ &= h(\alpha x + \Delta x) + \sqrt{h(\alpha x + \Delta x)}n_s + n_t + \Delta s, \end{aligned} \tag{3}$$

where h is the equivalent channel gain, $n_t \sim \mathcal{N}(0, \sigma_0^2)$ is the signal-independent thermal noise, $\sqrt{hs}n_s$ is the SDN with $n_s \sim \mathcal{N}(0, \eta^2\sigma_0^2)$, and Δs is the signal-independent nonlinear noise.

From (3), the SDN is related to signal x and distortion Δx. For a given data $\bar{x}$, the total noise variance in the received signal is given by

$$\begin{aligned}\mathbb{E}\{\sigma_n^2\} &= \mathbb{E}\left\{h(\alpha\bar{x} + \Delta x)\eta^2\sigma_0^2\right\} + \sigma_0^2 + \sigma_{\Delta s}^2 \\ &= h(\alpha\bar{x} + b)\eta^2\sigma_0^2 + \sigma_0^2 + \sigma_{\Delta s}^2, \end{aligned} \tag{4}$$

where $b = \mathbb{E}\{\Delta x|\bar{x}\}$. In (4), σ_0^2, $\sigma_{\Delta s}^2$ and $h(\alpha\bar{x} + b)\eta^2\sigma_0^2$ represent the thermal noise, nonlinear noise and signal-dependent noise, respectively. They are the main components of the VLC system noise.

C. Noise Strength in Nonlinear System

To determine whether SDN dominates, we define the ratio of SDN variance to SIDN variance as

$$\kappa = \frac{\sigma_{SDN}^2}{\sigma_{SIDN}^2} = \frac{h(\alpha\bar{x} + b)\eta^2\sigma_0^2}{\sigma_0^2 + \sigma_{\Delta s}^2}, \tag{5}$$

where $\sigma_{SDN}^2 = h(\alpha\bar{x} + b)\eta^2\sigma_0^2$ is the SDN variance and $\sigma_{SIDN}^2 = \sigma_0^2 + \sigma_{\Delta s}^2$ is the SIDN variance. Larger κ indicates more significant SDN in the system. It is clear that the value of κ is related to h, α and Δs. The impact of these factors on κ is investigated experimentally in the following section. Note that for a given detector, we assume that η and σ_0^2 are of fixed value, which is reasonable for practical applications.

On the other hand, when the incident optical power increases, the SDN in the APD output current can be approximated by a Gaussian random variable with variance [29]

$$\sigma_{SDN}^2 \approx 2qI_pBU^2E, \tag{6}$$

where q is the magnitude of the electronic charge, I_q is the photogenerated current, U is the APD multiplication factor, and $E = \rho U + (2 - \frac{1}{U})(1 - \rho)$ is the excess noise factor with ρ being the ionization ratio.

III. Experiments on SDN

A. Experimental Setup

To explore the SDN in the VLC system, we conduct several groups of comparative experiments, namely the case with linear transmitter and linear receiver (Case 1), the case with nonlinear transmitter and linear receiver (Case 2), the case with nonlinear transmitter and nonlinear receiver (Case 3), as illustrated in Fig. 2. The experimental scenario is shown in Fig. 3.

At the transmitter, the LED is driven by a Bias-Tee combining the DC bias from a DC power supply (Rigol DP832 A) with an AC signal from an arbitrary wave generator (AWG, Keysight 33612 A). Considering the non-ideal characteristics of Bias-Tee, we replace it with a switching circuit for comparison. The switching circuit is basically a switch that controls LED to transmit optical signal. Therefore, the switching circuit introduces negligible extra noise into the system. However, Bias Tee is an RC circuit that losses and distorts the input signal, which introduces nonlinearity into the system.

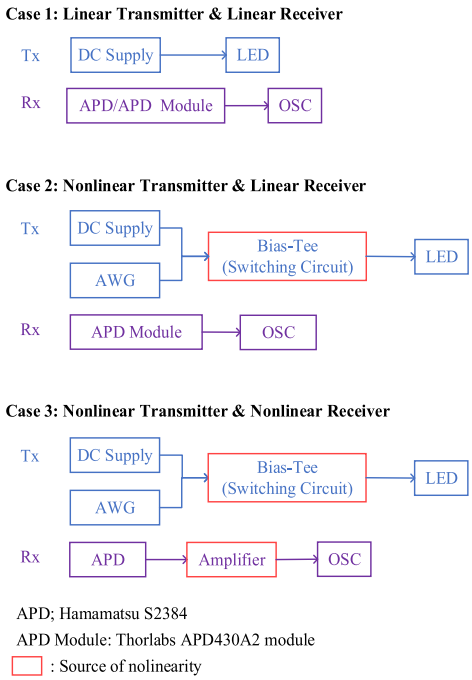

Fig. 2. Comparative experiments.

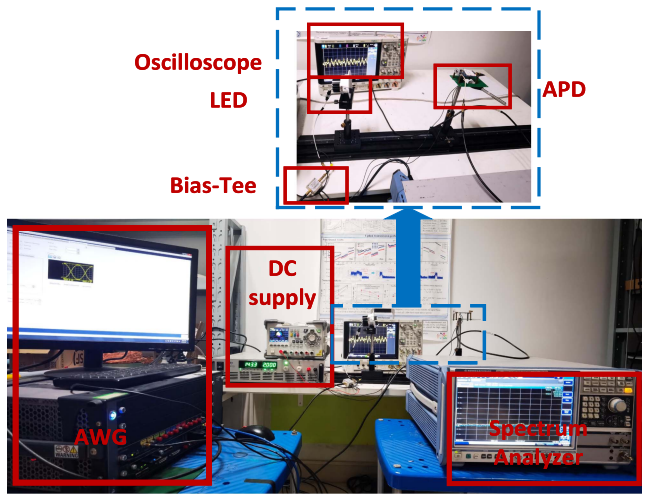

Fig. 3. Experimental scenario.

After passing through the channel, the optical signal is received by the APD. We adopt three types of APD receivers, including Hamamatsu S2384, Hamamatsu S2384 with amplifier circuit, and Thorlabs APD430A2 module. Note that due to different sensitive area sizes, the light intensities detected by APDs vary from one to another for the same transmitter. For the APD receiver of Hamamatsu S2384, we use spectrum analyzer to measure its weak output signal. For the other two types of APD receivers, we use Agilent Oscilloscope (OSC) to observe the waveform directly. In the experiment, the incident optical power at the receiver is measured by an optical power meter (Thorlabs PM100D with sensor S130 C).

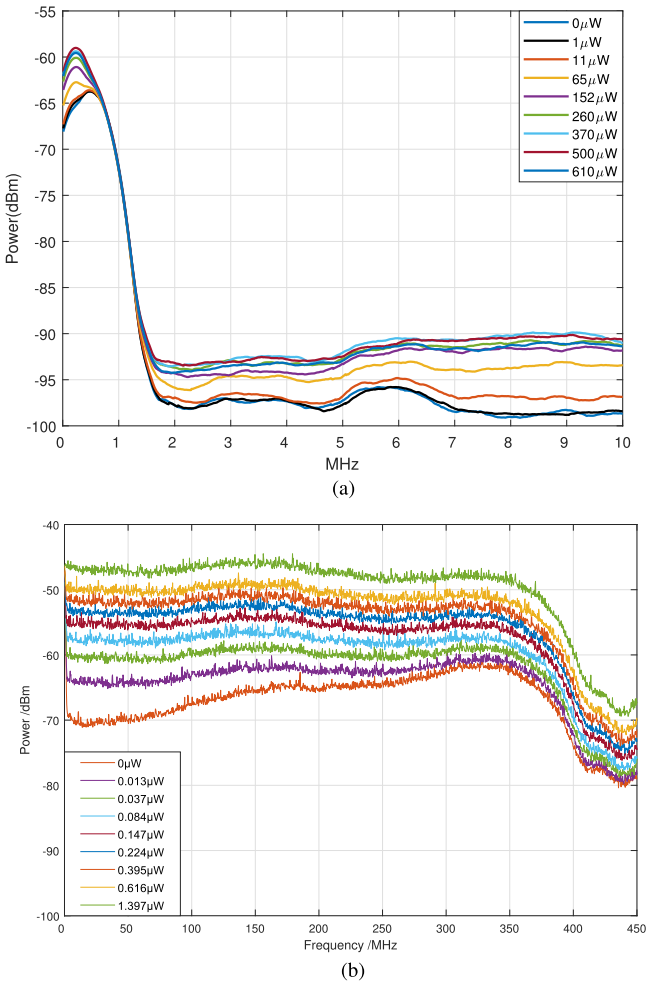

Fig. 4. Spectrum of APDs output with different incident light power. (a) Hamamatsu S2384. (b) Thorlabs APD430A2 module.

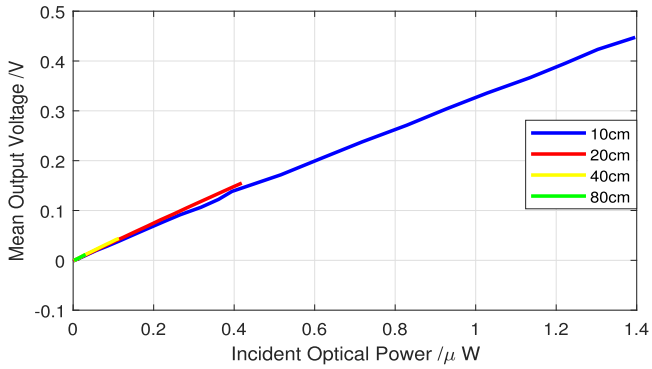

Fig. 5. Mean output voltage vs. incident optical power.

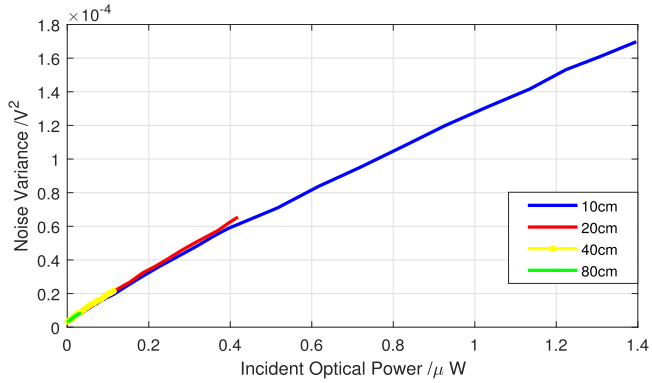

Fig. 6. Noise variance vs. incident optical power.

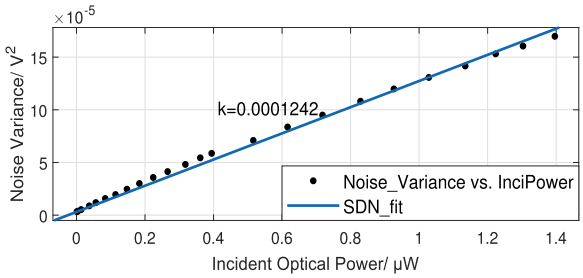

Fig. 7. Fitting curve of noise variance with respect to the incident optical power.

B. Case 1: Linear Transmitter and Linear Receiver

In this case, we only transmit DC signal and measure the noise at the receiver. The DC power supply, LED, APD and OSC are adopted in the experiment, where the least external noise is introduced. Consequently, the transmitter and receiver can both be considered linear in this scenario. The noise results using different receivers are as follows.

• *APD Hamamatsu S2384:* The spectrum of the APD Hamamatsu S2384 output signal with different incident light powers is shown in Fig. 4(a). Due to the inherent defects of the spectrum analyzer, the signal spectrum within the range of 0-2 MHz is not accurate. Therefore, we omit this component in the following analysis. From Fig. 4, we can clearly see that as the incident optical power increases, the output power becomes larger, indicating the existence of SDN. When the incident power is greater than 500 μW, the signal power spectrum tends to be stable due to the saturation effect of APD. Note that the output signal of APD Hamamatsu S2384 is extremely weak, an external amplifier is required in actual use, which introduces extra noise (cf. Case 3 in Section III-D).

• *Thorlabs APD430A2 module:* We conduct the test using Thorlabs APD430A2 module in the same environment as that for APD Hamamatsu S2384. The spectrum of the APD module output signal with different incident light powers is shown in Fig. 4(b). The noise variance also increases with the incident light power. The mean output voltage and noise variance with respect to the incident optical power are shown in Figs. 5 and 6, where different colored lines correspond to different transceiver distances. Fig. 7 shows the fitted line for the noise variance with slope $1.242e^{-4}$ and intercept $3.1e^{-6}$, from which the scaling factor can be calculated as $\eta^2 \approx 40$. The received signal waveforms with no light and $1.4\mu W$ incident optical power are shown in Fig. 8. It can be seen that SDN causes obvious fluctuations to the waveform under strong signal. Fig. 9 further shows the

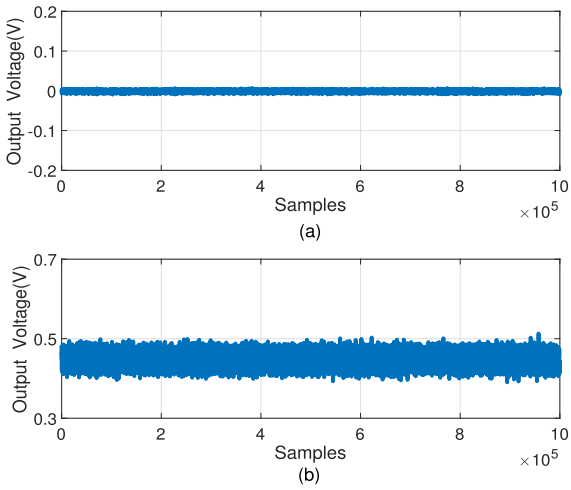

Fig. 8. Received signal waveforms. (a) No incident light. (b) $1.4\mu W$ incident optical power.

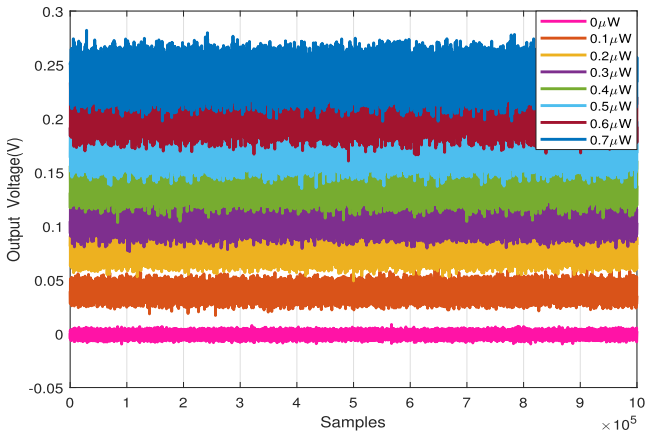

Fig. 9. Output signal waveforms with 0-0.7 μW incidental optical power.

received waveform with 0-0.7 μW optical power, where the noise variance increases with the intensity level. It also indicates the necessity of conducting modulation design.

Considering that the APD shot noise is the main source of SDN, we compare the experimental SDN variance with the theoretical shot noise variance given by (6). According to the device manual, the resistance of APD is 50 Ω, the bandwidth is 400 MHz, and the multiplication factor $U = 100$. The excess noise factor is set to be a classical value $E \approx 3.95$ [30]. The experimental curve is obtained by converting the output voltage into current and calculating the variance. Fig. 10 shows the theoretical and experimental shot noise variances under different incident optical powers with transceiver distance 10 cm. The theoretical and the experimental values are in the same order, only with a difference about 1.5 times, implying the same trend of the experimental values and the theoretical results. The mismatch between the theoretical values and experimental values can come from the parameter estimation errors (e.g., U fluctuates by $10\% - 15\%$).

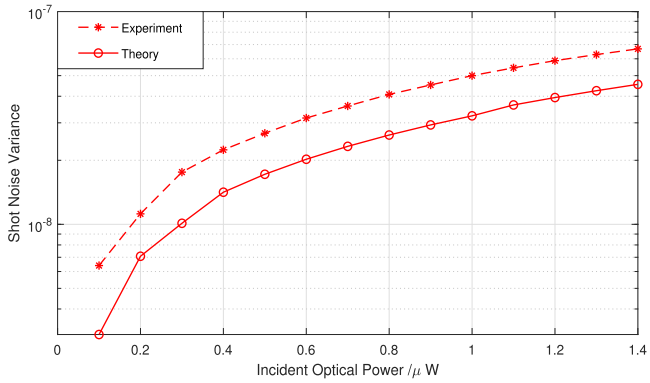

Fig. 10. Theoretical results and experimental results of the shot noise variance under different incident optical powers.

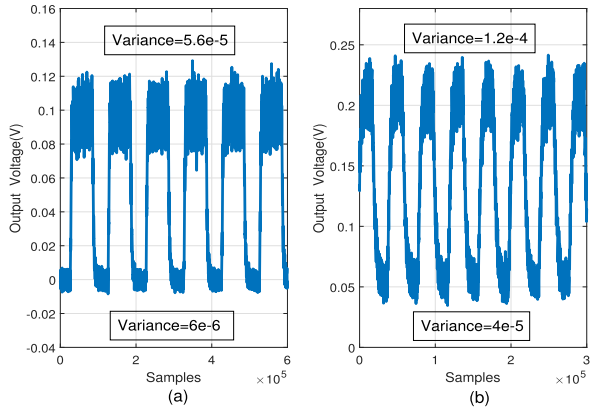

Fig. 11. Received signal waveforms by Thorlabs APD. (a) Utilizing the switching circuit. (b) Utilizing the Bias-Tee.

C. Case 2: Nonlinear Transmitter and Linear Receiver

In this subsection, we consider the case where DC and AC signals are combined by the signal coupler at the transmitter, and the optical signal is received by the Thorlabs APD430A2 module. The Bias-Tee at the transmitter will introduce nonlinearity, while the Thorlabs APD430A2 module at the receiver has a large linear range, which corresponds to the case with nonlinear transmitter and linear receiver. Here we use the switching circuit as a comparison to show the nonlinearity of Bias-Tee.

Fig. 11 shows the received signals when using the switching circuit and Bias-Tee under the same experimental conditions. It can be seen that when using the switching circuit, the amplitude fluctuation of symbol "1" is larger than that of symbol "0", indicating that the SDN dominates. When using Bias-Tee, the noise variance of symbol "0" increases significantly, reducing the gap of the noise variances corresponding to different symbols. This is because the switching circuit directly controls the light source on/off without introducing additional noise, while Bias-Tee deforms the waveform during signal coupling. Due to the device impairment, Bias-Tee introduces severe SIDN into the system, which makes SDN become insignificant.

Fig. 12 shows the mean and variance of received signal waveforms utilizing the Bias-Tee versus the peak-to-peak voltage (Vpp). It can be seen that the noise variance increases

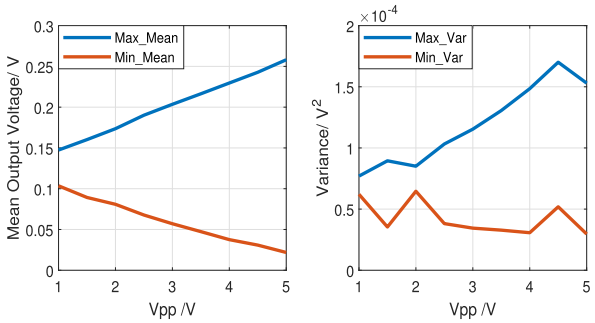

Fig. 12. Mean and variance of the received signal waveform utilizing the Bias-Tee and Thorlabs APD430A2 module vs. the transmitted Vpp.

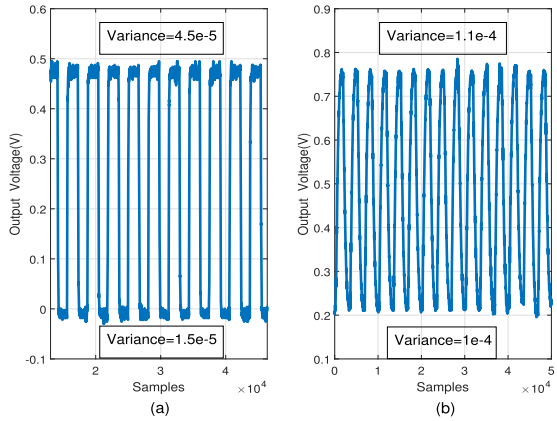

Fig. 13. Received waveform by APD Hamamatsu S2384. (a) Utilizing the switching circuit. (b) Utilizing the Bias-Tee.

gradually with Vpp, indicating strong correlation between the noise variance and the signal strength.

D. Case 3: Nonlinear Transmitter and Nonlinear Receiver

In this subsection, we consider the case where DC and AC signals are combined by the signal coupler, and the optical signal is received by the APD Hamamatsu S2384 with amplifier circuit. The Bias-Tee at the transmitter and the amplifier circuit at the receiver are both nonlinear devices. Fig. 13 shows the receiver output waveforms when the transmitted DC and AC signals are coupled by the switching circuit/Bias-Tee.

Fig. 14 shows the variation in the noise variance ratio of symbol "1" and "0" with respect to the transmitted Vpp utilizing the Bias-Tee and APD Hamamatsu S2384. It is obvious that due to the non-linear devices at both the transmitter and receiver, the noise variance ratio of symbol "1" and "0" is less than 1 when the transmitted Vpp is small (e.g., 1 V and 1.5 V). This indicates the significant influence of system nonlinearity on the receiver noise, especially in scenarios of weak signal. Meanwhile, as the signal strength increases, the SDN increases, and nonlinear effect becomes less obvious.

E. Noise Analysis

In this subsection, the noise analysis is presented for the three experimental cases.

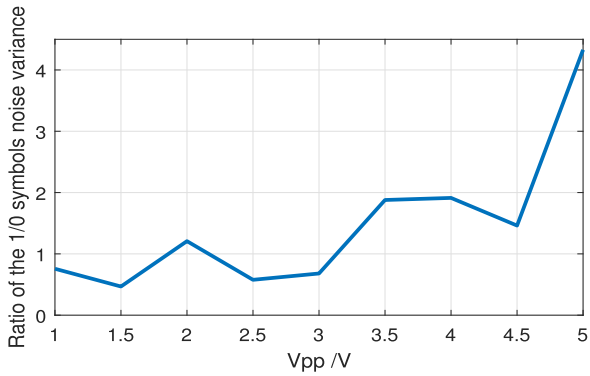

Fig. 14. Noise variance ratio of symbol "1" and "0" utilizing the Bias-Tee and APD Hamamatsu S2384 vs. the transmitted Vpp.

TABLE I
SUMMARY OF NONLINEARITY SOURCES

Nonlinearity source	Characteristic parameters	κ
None (Case 1)	$\alpha = 1, \Delta s = 0$	$h(\bar{x}+b)\eta^2$
Transmitter (Case 2)	$\alpha \neq 1, \Delta s = 0$	$h(\alpha\bar{x}+b)\eta^2$
Transmitter & Receiver (Case 3)	$\alpha \neq 1, \Delta s \neq 0$	$\frac{h(\alpha\bar{x}+b)\eta^2\sigma_0^2}{\sigma_0^2+\sigma_{\Delta s}^2}$

Case 1: It can be seen from the results in Section III-B that if there are highly linear devices (or the nonlinearity is weak), then $\alpha = 1, \Delta s = 0$, and κ can be simplified as $\kappa = h(\bar{x}+b)\eta^2$. The experimentally measured parameter scaling factor is $\eta^2 \approx 40$. When the received signal $h(\bar{x}+b) > 0.025\mu W$ (i.e., $\kappa > 1$), SDN will have a significant impact on the system performance. Such scenario is common when high-precision integrated devices are adopted at the transmitter and receiver. In this case, the SDN should be considered in the channel modeling. The traditional modulation design based on Euclidean distance will be inapplicable in this system, so a more suitable modulation scheme needs to be designed. For the static channel with constant link gain h, the noise variance increases monotonically with the signal strength.

Case 2: When there are only nonlinear devices at the transmitter, we have $\kappa = h(\alpha\bar{x}+b)\eta^2$, where $\alpha \neq 1$ is the attenuation factor depending on the output signal amplitude distortion of the nonlinear device. In this case, $\bar{x}$ and α determine the relative strength of SDN. For the devices with fixed α, the channel state can be considered the same as that in Case 1.

Case 3: When nonlinearity exists in both the transmitter and receiver devices, we have $\kappa = \frac{h(\alpha\bar{x}+b)\eta^2\sigma_0^2}{\sigma_0^2+\sigma_{\Delta s}^2}$, implying that κ approaches zero for weak signal (i.e., when SIDN is dominant in the system). In such scenario, the improved design of non-linear devices should be considered first, because large nonlinear noise make against high-speed communication.

Table I summarizes the above scenarios, including the difference in system noise. Considering the effect of SDN, the communication scheme needs to be designed in particular for high-precision VLC systems with low background noise, where SDN gradually dominates as the signal strength increases. If

there are non-ideal devices in the VLC system, which introduces nonlinear background noise, the SDN may not need to be prioritized.

IV. Modulation Optimization and Equalization for VLC System With SDN

A. Modulation Optimization

Due to the existence of SDN, the constellation design for minimizing SER cannot be approximated by that for maximizing the minimal constellation distance. In this subsection, we propose a constellation design method to minimize the SER under SDN.

Consider a VLC system employing M-PAM, where the transmitted symbol is chosen from constellation set $\mathcal{S} = \{s_1, s_2, \ldots, s_M\}$. Here we use the experimental results in Case 1 for the modulation design, and ignore the transmitter nonlinearity, i.e., $\alpha = 1$ and $\Delta x = 0$. The conditional probability density function of the received signal given transmitted symbol s_i is

$$P(y|s_i) = \frac{1}{\sqrt{2\pi}\sqrt{hs_i\eta^2\sigma_0^2 + \sigma_0^2}} \exp\left\{-\frac{(y-s_i)^2}{2(hs_i\eta^2\sigma_0^2 + \sigma_0^2)}\right\}. \tag{7}$$

Adopting the maximum likelihood (ML) detection, the transmitted symbol is determined as

$$\hat{i} = \arg \max_{1\le i\le N} p(y|s_i). \tag{8}$$

The most common modulation scheme is the uniform modulation, i.e., each constellation point is equally spaced. Since the noise power increases with the signal strength, we tend to keep larger space between symbols with higher power. Square-root modulation meets this requirement, but it is more suitable when SIDN is much smaller than SDN. For square-root modulation, the adjacent symbol amplitudes satisfy [31]

$$\sqrt{s_{i+1}} - \sqrt{s_i} = \beta, 1 \le i \le M-1, \tag{9}$$

where β is a parameter related to the modulation order. Combining the advantages of the uniform modulation and square-root modulation, we set the symbol amplitudes as linear weighted sums of the two constellations. The symbols in the combined modulation can be expressed as

$$L_{opt} = aL_{uni} + bL_{sqr}, \tag{10}$$

where a and b are the modulation coefficients, L_{uni} and L_{sqr} are the symbol amplitudes of the uniform and square-root modulations. To ensure a fixed peak power, we constrain $a + b = 1$. Take 4-PAM for example. With $L_{uni} = [0, 3, 6, 9]$ and $L_{sqr} = [0, 1, 4, 9]$, the optimized symbol amplitudes are $L_{opt} = [0, 3a + b, 6a + 4b, 9]$.

The optimal modulation coefficients a and b can be obtained by solving the following problem:

$$\begin{aligned} \min_{a,b} \quad & SER \\ \text{s.t.} \quad & L_{opt} = aL_{uni} + bL_{sqr} \\ & 0 \le a, b \le 1 \\ & a + b = 1. \end{aligned} \tag{11}$$

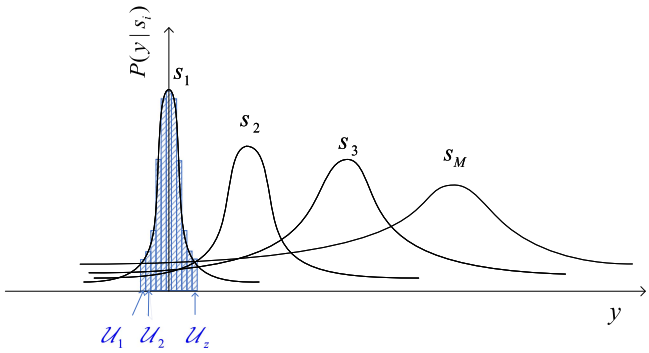

Fig. 15. Schematic diagram of the symbol decision region.

In order to obtain a theoretically optimal a, we implement an alternative algorithm. For M-PAM, the constellation of uniform and square-root modulations are $L_{uni} = [0, \frac{P}{(M-1)}, \frac{2P}{(M-1)}, \ldots, P]$, $L_{sqr} = [0, \frac{P}{(M-1)^2}, \frac{4P}{(M-1)^2}, \ldots, P]$, so the proposed constellation is $L_{opt} = [0, a \cdot \frac{P}{(M-1)^2} + (1-a) \cdot \frac{P}{(M-1)^2}, a \cdot \frac{4P}{(M-1)^2} + (1-a) \cdot \frac{4P}{(M-1)^2}, \ldots, P]$, where P is the peak power. The probability of detection error P_e is written as

$$P_{ei} = 1 - \int_{y\in\mathcal{D}_i} p(y|s_i)dy, i = 1, 2, \ldots, M, \tag{12}$$

where $\mathcal{D}_i$ is the decision region for symbol s_i.

Fig. 15 shows a schematic diagram of the symbol decision region. By discretizing the value range of received signal, we can obtain that

$$\mathcal{D}_1 = \mathcal{U}_1 \bigcup \mathcal{U}_2 \bigcup \cdots \bigcup \mathcal{U}_z. \tag{13}$$

The decision region of other constellation points can be similarly obtained. Note that the variances of symbols are different, any two probability density function (PDF) curves may have one or two intersections.

For a given a, the decision region of the constellation is fixed, and the P_e can be calculated accordingly by (12). Therefore, we can search for a in the range of [0,1] to obtain the theoretical optimal value.

B. LMMSE Equalization

In VLC system, the low-pass characteristic of LED results in ISI and degrades the detection performance at the receiver [32]. To suppress ISI, we perform linear equalization in VLC system with SDN.

In the presence of ISI, the received discrete-time signal at time n is

$$y(n) = \sum_{k=0}^{K} h(k)s(n-k) + \sqrt{\sum_{k=0}^{K} h(k)s(n-k)n_s(n) + n_t(n)}, \tag{14}$$

where K is the maximum delay. Here we employ the parameters obtained in the experiment of Case 1.

Denoting $\boldsymbol{y} = [y(n+K), y(n+K-1), \ldots, y(n)]^T$ and $\boldsymbol{s} = [s(n+K), s(n+K-1), \ldots, s(n-K)]^T$, we have

$$\boldsymbol{y} = \boldsymbol{H}\boldsymbol{s} + \mathrm{diag}(\sqrt{\boldsymbol{H}\boldsymbol{s}})\boldsymbol{n}_s + \boldsymbol{n}_t, \tag{15}$$

where $\boldsymbol{H}$ is a Toeplitz matrix with first row being $\boldsymbol{h}_{1r}^T = [h(0), h(1), h(2), \ldots, h(K), 0, \ldots, 0]$ and the first column being $\boldsymbol{h}_{1c} = [h(0), 0, \ldots, 0]^T$, $\boldsymbol{n}_s = [n_s(n+K), n_s(n+K-1), \ldots, n_s(n)]$ and $\boldsymbol{n}_t = [n_t(n+K), n_t(n+K-1), \ldots, n_t(n)]$.

We consider a linear equalization with L taps. To extract complete information from the received signal, L is typically greater than or equal to K. Here we assume $L = K$ for simplicity. Then, the estimate of symbol $s(n)$ is expressed as

$$\hat{s}(n) = \sum_{l=-L}^{0} w(l)y(n-l) + b = \boldsymbol{w}^T\boldsymbol{y} + b, \tag{16}$$

where $\boldsymbol{w} = [w(-L), w(-L+1), \ldots, w(0)]^T$ is the equalization vector, and b is a scalar.

We adopt the LMMSE equalization, where $\boldsymbol{w}$ and b are given by [33]

$$\boldsymbol{w}^T = \boldsymbol{R}_{sy}\boldsymbol{R}_{yy}^{-1}, \tag{17}$$

$$b = \mathbb{E}\{s(n)\} - \boldsymbol{w}^T\mathbb{E}\{\boldsymbol{y}\}, \tag{18}$$

where $\boldsymbol{R}_{sy}$ is the cross-covariance vector of $s(n)$ and $\boldsymbol{y}$; $\boldsymbol{R}_{yy}$ is the covariance matrix of $\boldsymbol{y}$. Matrices $\boldsymbol{R}_{sy}$ and $\boldsymbol{R}_{yy}$ can be further represented as

$$\begin{aligned}
\boldsymbol{R}_{sy} &= \mathbb{E}\{(s(n) - \mathbb{E}\{s(n)\})(\boldsymbol{y} - \mathbb{E}\{\boldsymbol{y}\})^T\} \\
&= \mathbb{E}\{s(n)\boldsymbol{y}^T\} - \mathbb{E}\{s(n)\}\mathbb{E}\{\boldsymbol{y}^T\} \\
&= \mathbb{E}\{s(n)[\boldsymbol{h}_{K+1c}s(n) + \sum_{i=1, i\neq K+1}^{2K+1} \boldsymbol{h}_{ic}s(n-K-1+i) \\
&\quad + \mathrm{diag}(\sqrt{\boldsymbol{H}\boldsymbol{s}})\boldsymbol{n}_s + \boldsymbol{n}_t]^T\} - \mathbb{E}\{s(n)\}\mathbb{E}\{[\boldsymbol{H}\boldsymbol{s} \\
&\quad + \mathrm{diag}(\sqrt{\boldsymbol{H}\boldsymbol{s}})\boldsymbol{n}_s + \boldsymbol{n}_t]^T\} \\
&= \mathbb{D}\{s(n)\}\boldsymbol{h}_{K+1c}^T + \mathbb{E}^2\{s(n)\}\sum_{i=1}^{2K+1}\boldsymbol{h}_{ic}^T \\
&\quad - \mathbb{E}\{s(n)\}\mathbb{E}\{\boldsymbol{s}^T\}\boldsymbol{H}^T \\
&= \mathbb{D}\{s(n)\}\boldsymbol{h}_{K+1c}^T,
\end{aligned} \tag{19}$$

$$\begin{aligned}
\boldsymbol{R}_{yy} &= \mathbb{E}\{(\boldsymbol{y} - \mathbb{E}\{\boldsymbol{y}\})(\boldsymbol{y} - \mathbb{E}\{\boldsymbol{y}\})^T\} \\
&= \mathbb{E}\{\boldsymbol{y}\boldsymbol{y}^T\} - \mathbb{E}\{\boldsymbol{y}\}\mathbb{E}\{\boldsymbol{y}^T\} \\
&= \mathbb{E}\{[\boldsymbol{H}\boldsymbol{s} + \mathrm{diag}(\sqrt{\boldsymbol{H}\boldsymbol{s}})\boldsymbol{n}_s + \boldsymbol{n}_t][\boldsymbol{H}\boldsymbol{s} + \mathrm{diag}(\sqrt{\boldsymbol{H}\boldsymbol{s}})\boldsymbol{n}_s \\
&\quad + \boldsymbol{n}_t]^T\} - \boldsymbol{H}\mathbb{E}\{\boldsymbol{s}\}\mathbb{E}\{\boldsymbol{s}^T\}\boldsymbol{H}^T \\
&= \mathbb{D}\{\boldsymbol{s}\}\boldsymbol{H}\boldsymbol{H}^T + \eta^2\sigma_0^2\mathbb{E}\{\mathrm{diag}(\boldsymbol{H}\boldsymbol{s})\} + \sigma_0^2\boldsymbol{I} \\
&= \mathbb{D}\{\boldsymbol{s}\}\boldsymbol{H}\boldsymbol{H}^T + \eta^2\sigma_0^2\mathbb{E}\{s\}\mathrm{diag}(\boldsymbol{H}\cdot\boldsymbol{1}) + \sigma_0^2\boldsymbol{I}.
\end{aligned} \tag{20}$$

In the M-level uniform modulation with peak power P, we have $\mathbb{E}\{s(n)\} = \frac{P}{2}$ and $\mathbb{D}\{s(n)\} = \frac{MP^2+P^2}{12(M-1)}$. Then, (19) and (20) can be rewritten as

$$\begin{aligned}
\boldsymbol{R}_{sy} &= \frac{MP^2+P^2}{12(M-1)}\boldsymbol{h}_{Kc}^T \\
\boldsymbol{R}_{yy} &= \frac{MP^2+P^2}{12(M-1)}\boldsymbol{H}\boldsymbol{H}^T + \left(\frac{\eta^2\sigma_0^2 P}{2}\sum_{i=0}^{K}h(i) + \sigma_0^2\right)\boldsymbol{I}.
\end{aligned} \tag{21}$$

It is worth noting that in the VLC system, the transmitted signal is non-negative, so the expectation $\mathbb{E}\{s(n)\}$ is not zero. Then, the LMMSE receiver can be expressed as

$$\hat{s}(n) = \mathbb{E}\{s(n)\} + \boldsymbol{R}_{sy}\boldsymbol{R}_{yy}^{-1}(\boldsymbol{y} - \mathbb{E}\{\boldsymbol{y}\}). \tag{22}$$

In the VLC system with SDN, we explore whether the root mean square error (RMSE) of the equalizer output is signal-dependent. We successively change the modulation amplitude of transmitted signal to obtain the corresponding estimation RMSE as

$$RMSE = \sqrt{\mathbb{E}\{|s(n) - \hat{s}(n)|^2\}}|_{s(n)=s_i, i=1,\ldots,M}. \tag{23}$$

C. Simulation Results and Analysis

In this subsection, we study the SER performance of the proposed method in both flat and ISI channels. The system parameters for simulation are set as the experimental data obtained in Section III-B.

With $a + b = 1$, the optimal solution to Problem (11) can be obtained via one-dimensional search for $a \in [0, 1]$. In our simulations, the exhaustive search for coefficient a is performed with step size 0.01. Note that the proposed modulations with $a = 0$ and $a = 1$ correspond to the uniform and square-root modulations. Therefore, the obtained constellation will achieve a performance gain over the uniform and square-root modulations if the searching range contains $\{0, 1\}$.

The optimal coefficient a versus κ for different modulation orders is shown in Fig. 16. In the simulation, we divided the value range $[-\frac{P}{2}, \frac{3P}{2}]$ of the received signal into 10000 subregions. For different modulation orders, we present the optimal a within the range of κ satisfying $P_e \geq 10^{-15}$. We can see that

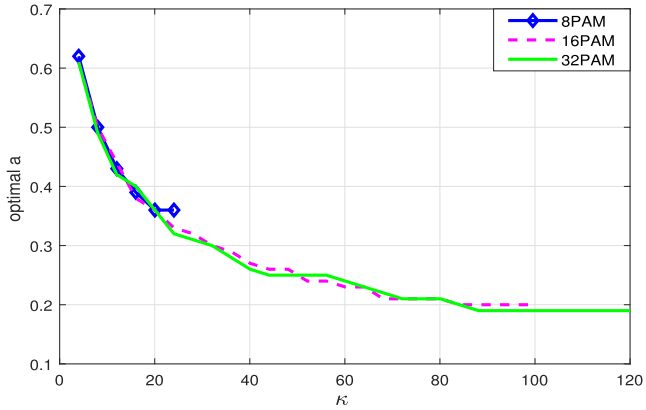

Fig. 16. Optimal a vs. κ for different modulation orders.

the optimal a converges to 0.36 for 8-PAM (or 0.2 for others) in the simulation results.

Remark 1: The optimal coefficients are related to the addictive noise of the environment. If there is a slight change in environmental conditions, we can adaptively adjust the coefficients following the rules in Fig. 16. If the environment changes dynamically, a real-time optimization design can be carried out.

For comparison, we also consider the optimal $M-$PAM constellations minimizing the SER, which corresponds to the following problem:

$$\begin{aligned} \min_{\mathcal{S}} \quad & SER \\ \text{s.t.} \quad & 0 = s_1 < s_2 < \cdots < s_M = P. \end{aligned} \tag{24}$$

However, it is hardly to obtain the global optimal solution due to the non-convexity of problem (24). Hence, we adopt the gradient descent method, the same as in [14], to solve this problem.

Fig. 17 shows the SERs of different modulation schemes versus κ with different modulation levels. The proposed modulation, uniform modulation, square-root modulation and the modulation scheme obtained by gradient descent method are labeled as "proposed", "uniform", "sqrt" and "suboptimal", respectively. Because the OOK and 4-PAM constellations of uniform modulation yield SER lower than 10^{-6} in the considered range of signal strength, we do not perform modulation optimization for $M = 2$ and $M = 4$. From Fig. 17(a)–(c), we can see that the proposed modulation scheme yields the lowest SER.

It can be seen that the "suboptimal" scheme does not always perform better than the uniform modulation. On the one hand, the performance of gradient descent method is closely related to the selection of initial points and parameters. On the other hand, the high dimension of the modulation vector leads to difficulty in the algorithm convergence.

Parameter κ characterizes the SDN strength, which is proportional to the incident optical power of APD. When using detectors with different diameters, the equivalent incident optical power of the detector can be converted from the measured value by optical power meter and the detector diameter. We use a $\phi 9.5$ mm optical power meter to measure the incident optical power at transmission distances of 1 m, 2 m and 3 m. The conversion results are marked with black arrows in Fig. 17(c), where d is the transmission distance. In different situations, an appropriate modulation scheme can be selected to improve the communication performance.

As for given κ, the variance of SIDN also affects the modulation performance. We set the σ^2_{SIDN} to be 10 times as the experimental value ($3.1e^{-6}$), and the SDN variance increases by 10 times accordingly to keep κ within a fixed range. That means greater distortion is introduced for the same signal amplitude. The SER results are shown in Fig. 18, where the square-root modulation is better than uniform modulation in this situation.

For simplicity, we consider three types of ISI channels:

$$\begin{aligned} h(n) &= 1 \\ h(n) &= 0.9 + 0.1n^{-1} \\ h(n) &= 0.8 + 0.1n^{-1} + 0.1n^{-2}, \end{aligned} \tag{25}$$

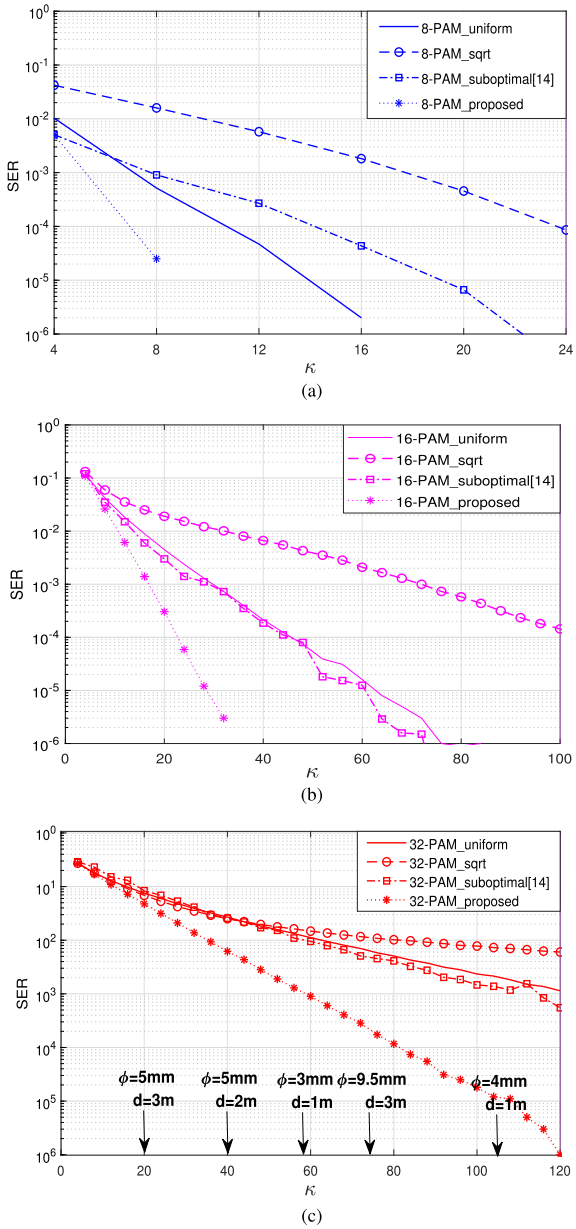

Fig. 17. SERs of different modulation schemes vs. κ with different modulation levels. (a) 8-PAM. (b) 16-PAM. (c) 32-PAM.

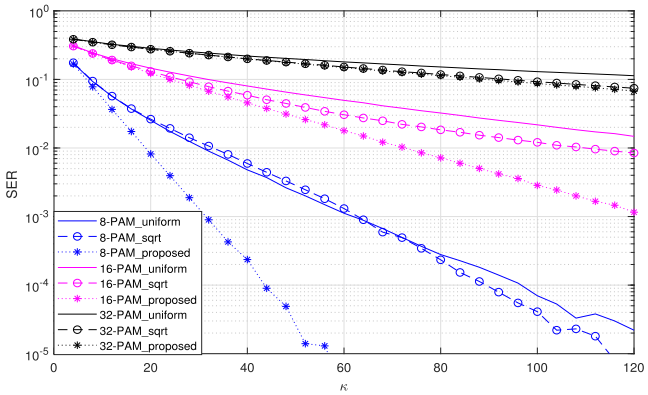

Fig. 18. SERs of different modulation schemes vs. κ when $\sigma^2_{SIDN} = 3.1e^{-5}$.

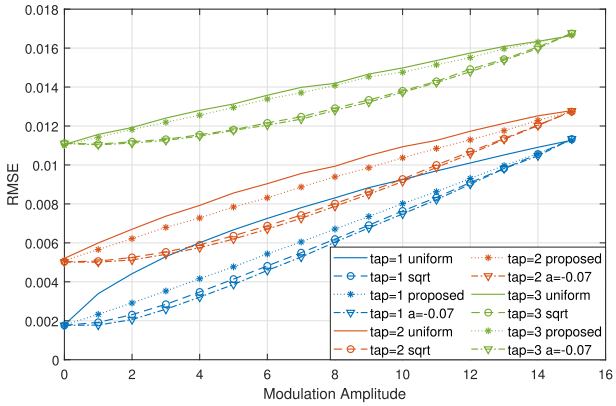

Fig. 19. RMSE under different modulation amplitude.

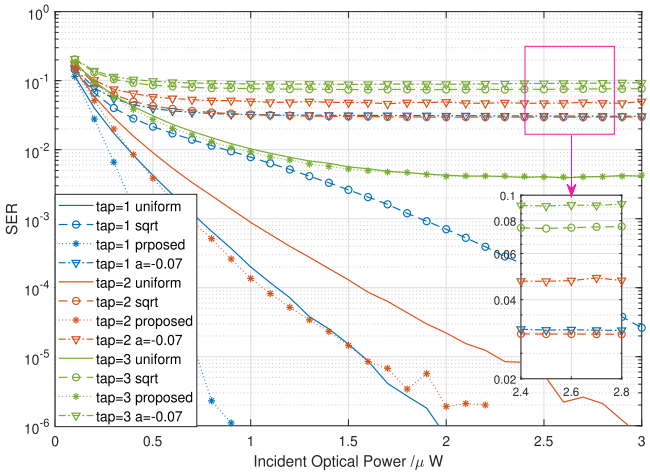

Fig. 20. SER vs. the incident optical power.

and represent them as "tap = 1", "tap = 2" and "tap = 3", respectively. We plot the RMSE of symbol estimation for 16-PAM in Fig. 19. As defined in (10), the uniform and square-root modulation schemes correspond to $a = 1$ and $a = 0$, respectively. We also perform parameter optimization for the three types of channels to minimize SER. To ensure that all symbol amplitudes are greater than or equal to 0, the minimum value of a is -0.07, which satisfies $aL_{uni} + (1-a)L_{sqr} \geq 0$. In Fig. 19, the RMSE of symbol estimation increases monotonically with the modulation amplitude because larger signal amplitude corresponds to larger SDN, which agrees with (22) and (23). The smallest RMSE of symbol estimation is achieved when the signal strength approaches zero and there is hardly any stimulated SDN in the system.

The corresponding SER curve for the ISI channel is shown in Fig. 20. It can be seen that the SER increases with the interference. When tap = 3, the curves of the optimized modulation and uniform modulation are roughly in coincidence, indicating that the uniform modulation is less sensitive to interference than the square-root modulation. It is worth noting that the combined modulation with $a = -0.07$ leads to lower RMSE of symbol estimation than the uniform modulation, but it is not optimal when taking SER into consideration. Due to the unequal transmission

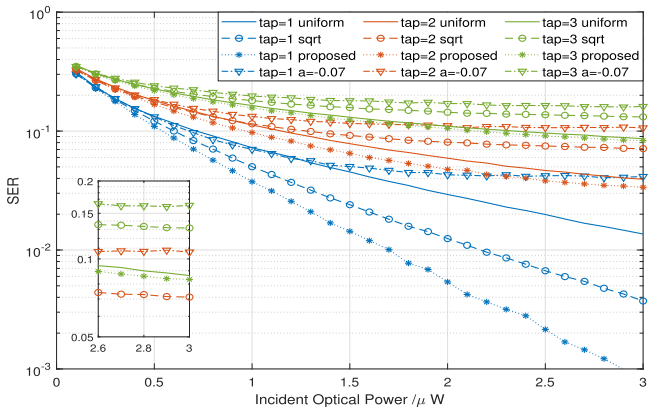

Fig. 21. SER vs. the incident optical power when $\eta^2 = 400$.

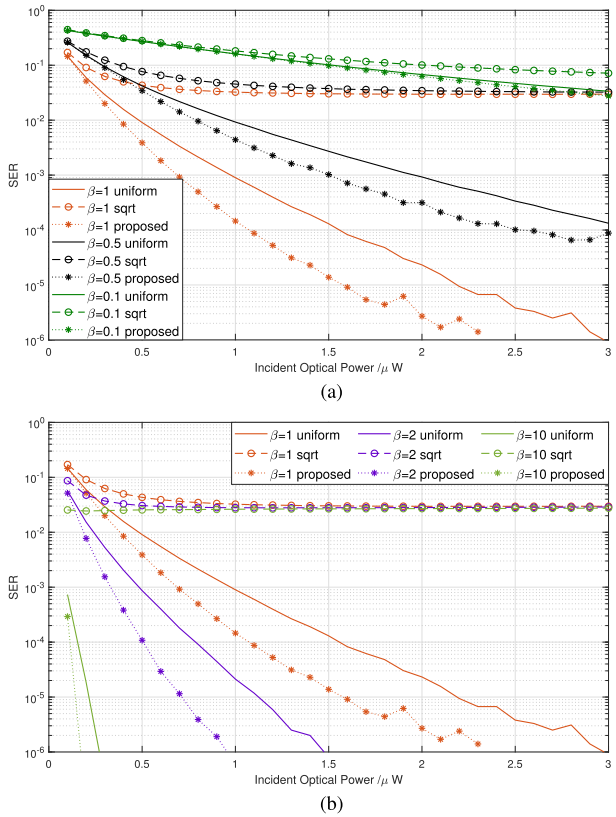

Fig. 22. SER vs. the incident optical power with different scale factors. (a) $\beta \leq 1$. (b) $\beta \geq 1$.

power of the two methods, a lower RMSE of symbol estimation does not indicate a higher SNR in such case.

Specially, when SDN is dominant in the system, the square-root modulation outperforms the uniform modulation in terms of RMSE and SER. For example, setting $\eta^2 = 400$ (10 times as the Thorlabs APD430A2 module), the RMSE and SER are shown in Fig. 21 .

We also study the sensitivity of the optimized modulation parameters in other ISI cases. We multiply $h(n)$ by a scale factor β to represent ISI channels at different transmission distances, the SER corresponding to $\beta(0.9 + 0.1n^{-1})$ is shown in Fig. 22.

It is seen that the optimized modulation leads to the smallest SER in different cases, indicating that the modulation parameters are insensitive to the ISI environment.

V. Conclusion

In this article, we have explored the SDN in nonlinear VLC systems by several comparative experiments. Experimental results verify the existence of SDN in VLC systems, but non-ideal devices such as Bias-Tee and amplifier can introduce additional noise, making it difficult to observe SDN. Based on the model of nonlinear VLC system, the SDN strength is related to device nonlinearity and signal amplitude. We have also investigated the modulation optimization and LMMSE equalization for VLC systems with SDN. Simulation results have shown that the SER is significantly reduced by the optimized modulation in flat channel. Adopting LMMSE equalization, the RMSE of symbol estimation increases monotonically with the modulation amplitude in the presence of SDN. Moreover, the optimized modulation also outperforms the uniform modulation in the ISI channel, and is insensitive to the interference intensity.

References

[1] Z. Xu, W. Liu, Z. Wang, and L. Hanzo, "Petahertz communication: Harmonizing optical spectra for wireless communications," *Digit. Commun. Netw.*, vol. 7, no. 4, pp. 605–614, Nov. 2021.

[2] L. E. M. Matheus, A. B. Vieira, L. F. Vieira, M. A. Vieira, and O. Gnawali, "Visible light communication: Concepts, applications and challenges," *IEEE Commun. Surveys Tuts.*, vol. 21, no. 4, pp. 3204–3237, Fourth Quarter 2019.

[3] J. Wang, J. Wang, and Y. Wang, "Fundamental analysis for visible light communication with input-dependent noise," in *Optical Fiber and Wireless Communications*. Rijeka, Croatia: IntechOpen, 2017, pp. 143–157.

[4] Q. Gao, K. Qaraqe, and E. Serpedin, "Rotated color shift keying for visible light communications with signal-dependent noise," *IEEE Commun. Lett.*, vol. 24, no. 4, pp. 844–848, Apr. 2020.

[5] A. Cheema, M. Alsmadi, and S. Ikki, "Distance estimation in visible light communications: The case of imperfect synchronization and signal-dependent noise," *IEEE Trans. Veh. Technol.*, vol. 70, no. 10, pp. 11044–11049, Oct. 2021.

[6] M. Yaseen, M. Alsmadi, A. E. Canbilen, and S. S. Ikki, "Visible light communication with input-dependent noise: Channel estimation, optimal receiver design and performance analysis," *J. Lightw. Technol.*, vol. 39, no. 23, pp. 7406–7416, Dec. 2021.

[7] M. Yuan, X. Sha, X. Liang, M. Jiang, J. Wang, and C. Zhao, "Coding performance for signal dependent channels in visible light communication system," in *Proc. IEEE Glob. Conf. Signal Inf. Process.*, 2015, pp. 1037–1041.

[8] S. M. Moser, "Capacity results of an optical intensity channel with input-dependent Gaussian noise," *IEEE Trans. Inf. Theory*, vol. 58, no. 1, pp. 207–223, Jan. 2012.

[9] J.-Y. Wang, X.-T. Fu, R.-R. Lu, J.-B. Wang, M. Lin, and J. Cheng, "Tight capacity bounds for indoor visible light communications with signal-dependent noise," *IEEE Trans. Wireless Commun.*, vol. 20, no. 3, pp. 1700–1713, Mar. 2020.

[10] H. Ghourchian, G. Aminian, A. Gohari, M. Mirmohseni, and M. Nasiri-Kenari, "On the capacity of a class of signal-dependent noise channels," *IEEE Trans. Inf. Theory*, vol. 64, no. 12, pp. 7828–7846, Dec. 2018.

[11] A. Elmoslimany and T. M. Duman, "On the discreteness of capacity-achieving distributions for fading and signal-dependent noise channels with amplitude-limited inputs," *IEEE Trans. Inf. Theory*, vol. 64, no. 2, pp. 1163–1177, Feb. 2018.

[12] T. Pfau, X. Liu, and S. Chandrasekhar, "Optimization of 16-ary quadrature amplitude modulation constellations for phase noise impaired channels," in *Proc. Eur. Conf. Expo. Opt. Commun.*, Optica Publishing Group, 2011, Paper Tu.3.A.6.

[13] J. Shi, J. Cai, G. Qin, R. Jin, X. Lin, and N. Chi, "Geometrically shaped 32QAM and modified binary switching coding method in underwater visible light communication," *Chin. J. Electron.*, vol. 31, no. 6, pp. 1106–1111, Nov. 2022.

[14] Q. Gao, S. Hu, C. Gong, and Z. Xu, "Modulation designs for visible light communications with signal-dependent noise," *J. Lightw. Technol.*, vol. 34, no. 23, pp. 5516–5525, Oct. 2016.

[15] Q. Gao, S. Hu, C. Gong, E. Serpedin, K. Qaraqe, and Z. Xu, "Distance-range-oriented constellation design for VLC-SCMA downlink with signal-dependent noise," *IEEE Commun. Lett.*, vol. 23, no. 3, pp. 434–437, Mar. 2019.

[16] Q. Gao, K. Qaraqe, and E. Serpedin, "Improving the modulation designs for visible light communications with signal-dependent noise," *IEEE Commun. Mag.*, vol. 58, no. 5, pp. 26–32, May 2020.

[17] H. Chen and Z. Xu, "A two-dimensional constellation design method for visible light communications with signal-dependent shot noise," *IEEE Commun. Lett.*, vol. 22, no. 9, pp. 1786–1789, Sep. 2018.

[18] M. Laakso, A. A. Dowhuszko, and R. Wichman, "Empirical evaluation of OFDM waveforms for VLC in the presence of LED nonlinearities," in *Proc. IEEE 32nd Annu. Int. Symp. Pers. Indoor Mobile Radio Commun.*, 2021, pp. 465–470.

[19] M. Gao, C. Li, and Z. Xu, "Optimal transmission of VLC system in the presence of LED nonlinearity and APD module saturation," *IEEE Photon. J.*, vol. 10, no. 5, pp. 1–14, Sep. 2018.

[20] H. Elgala, R. Mesleh, and H. Haas, "An LED model for intensity-modulated optical communication systems," *IEEE Photon. Technol. Lett.*, vol. 22, no. 11, pp. 835–837, Jun. 2010.

[21] S. Mardanikorani, X. Deng, and J.-P. M. Linnartz, "Optimization and comparison of M-PAM and optical OFDM modulation for optical wireless communication," *IEEE Open J. Commun. Soc.*, vol. 1, pp. 1721–1737, Oct. 2020.

[22] K. Ikeda, S. Horiuchi, T. Tanaka, and W. Susaki, "Design parameters of frequency response of GaAs–(Ga, Al) As double heterostructure LED's for optical communications," *IEEE Trans. Electron Devices*, vol. 24, no. 7, pp. 1001–1005, Jul. 1977.

[23] R. Mitra and V. Bhatia, "Chebyshev polynomial-based adaptive predistorter for nonlinear LED compensation in VLC," *IEEE Photon. Technol. Lett.*, vol. 28, no. 10, pp. 1053–1056, May 2016.

[24] M. Zhang et al., "4.05-Gb/s RGB LED-based VLC system utilizing PS-Manchester coded Nyquist PAM-8 modulation and hybrid time-frequency domain equalization," in *Proc. OSA Opt. Fiber Commun. Conf.*, 2017, pp. 1–3.

[25] T.-K. Nguyen, C.-H. Kim, G.-J. Ihm, M.-S. Yang, and S.-G. Lee, "CMOS low-noise amplifier design optimization techniques," *IEEE Trans. Microw. Theory Techn.*, vol. 52, no. 5, pp. 1433–1442, May 2004.

[26] H. T. Friis, "Noise figures of radio receivers," *Proc. IRE*, vol. 32, no. 7, pp. 419–422, Jul. 1944.

[27] W. R. Bennett, "Spectra of quantized signals," *Bell Syst. Tech. J.*, vol. 27, no. 3, pp. 446–472, Jul. 1948.

[28] O. T. Demir and E. Bjornson, "The Bussgang decomposition of nonlinear systems: Basic theory and MIMO extensions [lecture notes]," *IEEE Signal Process. Mag.*, vol. 38, no. 1, pp. 131–136, Jan. 2021.

[29] W. Liu and Z. Xu, "APD nonlinearity and its impact on PAM-based visible light communication," *IEEE Commun. Lett.*, vol. 24, no. 5, pp. 1057–1061, May 2020.

[30] PerkinElmer, "Avalanche photodiode: A user guide," [Online]. Available: https://resources.perkinelmer.com/corporate/cmsresources/images/44-6538app_avalanchephotodiodesusersguide.pdf/

[31] C. Gong, Q. Gao, and Z. Xu, "Analysis and design of amplitude modulation for optical wireless communication with shot noise," in *Proc. IEEE Int. Conf. Commun.*, 2016, pp. 1–6.

[32] J. Lian, M. Noshad, and M. Brandt-Pearce, "Comparison of optical OFDM and M-PAM for LED-based communication systems," *IEEE Commun. Lett.*, vol. 23, no. 3, pp. 430–433, Mar. 2019.

[33] S. M. Kay, *Fundamentals of Statistical Signal Processing: Estimation Theory*. Hoboken, NJ, USA: Prentice-Hall, 1993.